Progress In Electromagnetics Research C, Vol. 68, 153–161, 2016

A Novel Low RCS Microstrip Antenna Array Using Thin and Wideband Radar Absorbing Structure Based on Embedded Passives Resistors

Madhu A. Ramkumar[1], Chandrika Sudhendra[1, *], and Kark Rao[2]

Abstract—A novel low radar cross section (RCS) microstrip patch antenna array (1×4) (MSPAA) is reported in this paper. A thin and wideband radar absorber (RA) based on a single octagonal loop (SOL) resistive frequency selective surface (FSS) is designed for realizing out-of-band RCS reduction of the MSPAA from 6.2 GHz to 18 GHz. The RA is designed for −15 dB reflectivity from 6.2 GHz to 18 GHz. Embedded Passives (EP) resistors are used for implementing the resistors as integral to the substrate with no soldering at all which results in a quantum improvement in reliability. Full wave analysis of the low RCS MSPAA with the RA is carried out using HFSS. RCS measurements are performed, and an RCS reduction of 6 to 18 dB is attained compared to the reference antenna array over a wide band from 6 GHz to 18 GHz, with no degradation in VSWR and gain of the antenna array. The thin and wideband RA with its low weight and flight worthy constituent materials can be applied independently as skins of a stealthy UAV configured primarily for low RCS with external shaping, and the proposed antenna array can be used without modifications, as a low RCS conformal antenna structure.

1. INTRODUCTION

Microstrip antennas on board an air vehicle platform designed primarily for stealth contribute significantly to the overall radar cross section (RCS). Design of a low observable platform for realizing radar stealth includes the primary external shape design for monostatic radar cross section reduction (RCSR) and application of radar absorbers [1–7] which need to be designed and integrated as robust load bearing radar absorbing structures (RAS). Radar absorbers such as Salisbury screen [1], Jaumann RA [2–4] and different types of circuit analog absorbers [5–7] have been reported in open literature for realizing RCSR.

Antenna RCS [8] is defined as

$$\sigma = \left|\sqrt{\sigma_s} - (1-\Gamma_A)\sqrt{\sigma_r}e^{i\varphi}\right|^2 \tag{1}$$

where, $\boldsymbol{\sigma}$ is the total RCS of the target, $\boldsymbol{\sigma}_s$ related to the field scattered by the short-circuited antenna, $\boldsymbol{\sigma}_r$ the field scattered by the antenna that involves value of the port impedance, $\boldsymbol{\Gamma}_A$ the antenna reflection coefficient, and $\boldsymbol{\varphi}$ the relative phase between the two terms. Hence, RCS is the difference between two terms, one being the square root of a complex "structural" cross section and the other $(1 - \Gamma)$ times the square root of a complex "antenna" cross section.

Frequency selective surfaces (FSS) have been used in the ground plane as bandpass filters [9, 10], resulting in narrow out-of-band RCSR of the microstrip antenna, and band stop filters [11–13], other for achieving wide-band RCSR in out-of-band frequency regions of the antenna. Polarization dependent

Received 5 August 2016, Accepted 21 September 2016, Scheduled 18 October 2016

* Corresponding author: Chandrika Sudhendra (chandrika@ade.drdo.in).

[1] Aeronautical Development Establishment (ADE), Ministry of Defence, DRDO Bengaluru, India. [2] PES College of Engineering, Mandya, Karnataka, India.

FSS in the modified ground plane (MGP) for wide angle, in-band RCSR is reported in [14]. Fractal uniplanar compact ground is proposed in [15] for out-of-band structural RCSR. As low RCS antennas are a primary requirement of stealthy aircrafts/UCAVs, the FSS structures in the ground plane of an antenna on board a stealthy air vehicle loses its basic FSS characteristics attributed to unavailability of free space environment to the ground plane. This would result in degraded RCSR. Narrow-band, wide-band, dual-band, in-band and out-of-band RCSR of antenna, with either lower or increased gain using meta surfaces comprising EBG, AMC, lumped element loaded FSS is reported in [16–22] which results in either increased real estate of the antenna or the profile which would increase the aerodynamic drag on a stealthy air vehicle, limiting the application. Lumped element loading is used for realizing antenna RCSR in [16, 18, 19, 22, 23]. However, lumped resistors' loading is highly susceptible to soldering related defects and result in reduced reliability.

In this paper, RCSR of a microstrip patch antenna array (MSPAA) is described using a single octagonal loop resistive FSS based radar absorber. The novelty of the paper lies in the implementation of the low RCS MSPAA with absorber using embedded passives (EP) resistors, as a first time development in low RCS microstrip antennas, in open literature. The EP resistors are an enabling technology for implementing the resistive FSS layer of radar absorber for realizing the low RCS antenna as large number of resistors can be embedded without soldering, thus eliminating soldering related defects, reduced cross talk and parasitic reactance. RA design with full wave analysis using HFSS is described in the first section, and low RCS (1×4) MSPAA design is described next, followed by the design, simulation, fabrication and RCS measurements of the low RCS MSPAA. The RA is designed for reflectivity of -15 dB over 6.2 GHz to 16 GHz frequency bands and is realized as a thin and wideband Radar Absorbing structure (RAS). The low RCS antenna realized using the RA finds direct applications on any *stealth design driven* platform as a conformal stealthy structure where stealth design features such as external shaping and RA are already in place.

2. EM DESIGN AND FULL WAVE ANALYSIS OF RESISTIVE OCTAGONAL LOOP FSS ELEMENT BASED RADAR ABSORBER

The dielectric profile of the thin and wideband radar absorber (RA) shown in Fig. 1(a) comprises a superstrate top layer with the resistive FSS layer underneath, separated from the conducting ground plane by an RF transparent dielectric spacer. The superstrate layer is a 1.6 mm thick Rogers Ultralam 2000, with $\boldsymbol{\varepsilon}_r = 2.5$ and $\tan \boldsymbol{\delta} = 0.0019$. The crucial resistive FSS layer is conceptualized and designed using single octagonal loop (SOL) FSS geometry with resistors at the center of each side of the loop and is developed as a PCB using a 5 mils thick FR4 substrate. The resistors crucial for providing resistive loss are designed and implemented as EP resistors using a commercially available $50\,\Omega$/sq resistive sheet.

The total thickness of RA proposed in this paper is 5.6 mm (including superstrate thickness of 1.6 mm and dielectric spacer Rohacel foam thickness of 4 mm with $\boldsymbol{\varepsilon}_r = 1.07$ and $\tan \boldsymbol{\delta} = 0.0007$) used as the spacer between the resistive FSS layer and the conducting backplane and hence does not violate the fundamental minimum thickness constraint given by Rozanov in [24]. The design of RA lies in implementation of large number of resistors as EP resistors. The RA is modeled using transmission line (TL) equivalent circuit model and is given in Fig. 1(b). The resistive FSS layer is modeled as a series RLC circuit in shunt with the dielectric spacer backed conducting ground plane, acting as a short circuited transmission with length $<\boldsymbol{\lambda/4(d)}$, (where λ is the operating wavelength at the design center frequency, 11.75 GHz), and the grounded dielectric spacer terminated in short circuit is modeled as an equivalent inductance.

The surface impedance of FSS layer is given by:

$$Z_{FSS} = R_S + \frac{1}{j\omega C} + j\omega L \tag{2}$$

where, R is the surface resistance, C the capacitance and L the surface inductance of the FSS layer.

The free-space input impedance of RAM for normal incidence is given by:

$$Z_{in} = \frac{jZ_{FSS}Z\tan(\beta d)}{(Z_{FSS} + jZ\tan(\beta d))} \tag{3}$$

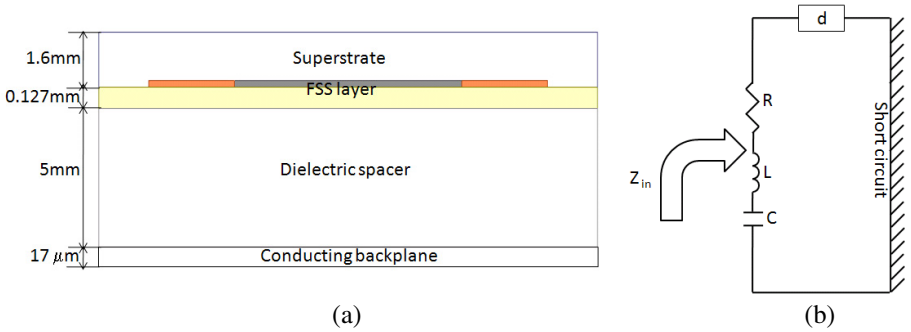

Figure 1. (a) Dielectric profile of thin and wideband RA. (b) Equivalent circuit model of resistive FSS layer of RA.

where, **Z** is the characteristic impedance of the PEC backed dielectric spacer, which behaves as an inductor (for sufficiently small thickness), and β is the propagation constant of the foam spacer material.

The free-space reflection coefficient, $\boldsymbol{\rho}$ of RAM at normal incidence is given by:

$$\rho = \frac{Y_{in} - Y_0}{Y_{in} - Y_0} \tag{4}$$

and reflectivity $\boldsymbol{\Gamma}$, by

$$\Gamma = 20\log_{10}(\rho) \tag{5}$$

where, Z_0 represents the impedance of free space and is equal to 377 Ω.

The SOL unit cell design details are shown in Fig. 2. The EP resistors at the center of each side of the SOL in a square lattice constitute the periodic resistive FSS layer of RA. The rotational symmetry of the SOL FSS geometry enables realization of polarization independent response. The dimensions of unit cell FSS are: $l = 10.39$ mm, $l_1 = 1.2$ mm, $l_2 = 3.06$ mm, $w_1 = 1$ mm and $w_2 = 1.5$ mm, where l is the length of the unit cell, l_1 the length of the EP resistor, l_2 the side length of SOL, w_1 the width of copper and also the EP resistor, and $(2w_2)$ the pitch of the unit cell.

As it is intended to design the RA for realizing polarization independent performance over ϕ varying from 0° to 90°, it is crucial that the geometry results in circularly polarized fields with "time and space quadrature" conditions. This is achieved by a judicious design of an octagonal FSS geometry, which enables realization of polarization independent RCSR performance from the RA. Compared to other CP enabling symmetrical FSS loop geometries such as square and hexagon, the octagonal FSS loop geometry with its longest perimeter results in lower coupling between cells. All design parameters of

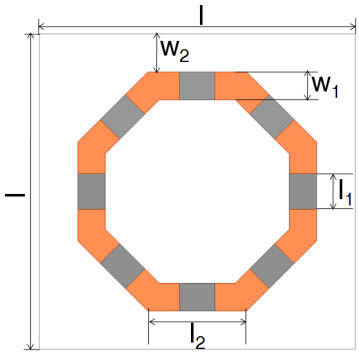

Figure 2. Design details of unit cell of resistive FSS.

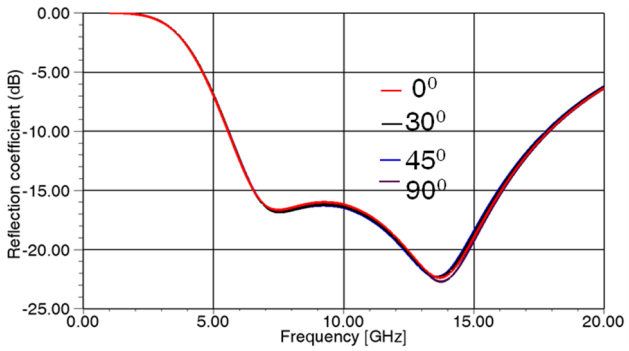

Figure 3. Simulated TE and TM reflectivity patterns of RAS for normal incidence with different polarization angles.

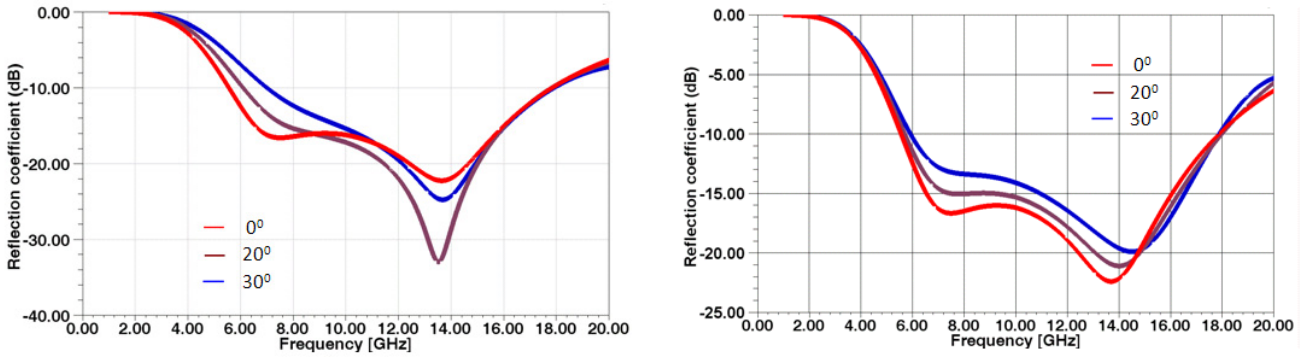

Figure 4. Reflectivity performance of RA with various angle of incidence. (a) TE incidence. (b) TM incidence.

the unit cell geometry are extracted using GA optimization in HFSS, with constraints in thickness for realizing the desired wideband RCSR performance.

A graph of optimized reflectivity performance vs. frequency is plotted in Fig. 3, for normal incidence. It is observed from the plot that a reflectivity/S_{11} of -10 dB (minimum) can be realized from 5.5 GHz to 18 GHz for both TE and TM incidences and indicates polarization independent performance of RA. Next, the RCSR performance of RA for non-normal angles of incidence is studied. Figs. 4(a) and 4(b) show the TM and TE performances of RA from 0° to 30°. It is observed from the figures that the -10 dB reflectivity performance of RA is preserved for angles of incidence up to 30°.

3. DESIGN AND FULL WAVE ANALYSIS OF LOW RCS MICROSTRIP ANTENNA ARRAY

A reference (1×4) element microstrip antenna array (MSPAA) for telemetry applications is designed at 2.25 GHz using an RT Duroid microwave substrate of size (300×98.75) mm^2, with relative permittivity, $\varepsilon_r = 2.5$, $\tan\boldsymbol{\delta} = 0.0019$ and thickness 1.6 mm. The dielectric profile of the low RCS MSPAA is shown in Fig. 5(a), and the schematic is shown in Fig. 5(b). The modified ground plane (MGP) of the reference MSPAA comprises solid copper ground *underneath the patches and the feed lines only*. The remaining area of the MGP layer is filled with octagonal resistive FSS elements, realized as a 5 mils thick FR4 PCB, referred to as the resistive FSS layer in the earlier section. The resistive FSS layer is spaced from the conducting ground plane by the RF transparent Rohacel foam layer of thickness 4 mm with $\varepsilon_r = 1.07$ and $\tan\boldsymbol{\delta} = 0.0007$. A thin tin-plated 3M copper foil is used as ground plane of the proposed low RCS MSPAA. The proposed low RCS antenna design is optimized in HFSS for realizing the desired performance, and the simulated S_{11} of the reference and proposed antenna are plotted in Fig. 6(a). The reference MSPAA is designed for a center frequency of 2.25 GHz with a bandwidth of 39 MHz. It is noted that with MGP, the center frequency shifts from 2.25 GHz to 2.23 GHz as shown in Fig. 6(a). By filling the resistive FSS elements around the MGP, the desired center frequency of 2.25 GHz is retrieved as the FSS elements act as PEC at 2.25 GHz, and the bandwidth of the proposed low RCS MSPAA is 43 MHz. The simulated gains of the reference and proposed low RCS MSPAA are 12 dBi in both E and H-planes, as shown in Figs. 6(b) and 6(c). It is observed that the *proposed low RCS MSPAA can be realized with no degradation in gain*. A very marginal increase in the back lobe is observed, and some side lobes are reduced.

Next, the structural RCS of the MSPAA is simulated in HFSS, and the results are plotted in Figs. 7(a) and (b). It is observed from the superposed plots that a 5 dB to 14 dB reduction in RCS is observed over a frequency range of 6 GHz to 18 GHz for both TE and TM incidences.

From the simulated radiation performance plots, it is observed that there is no degradation in gain, and the two graphs coincide.

The design of the low RCS MSPAA is optimized with the following considerations:

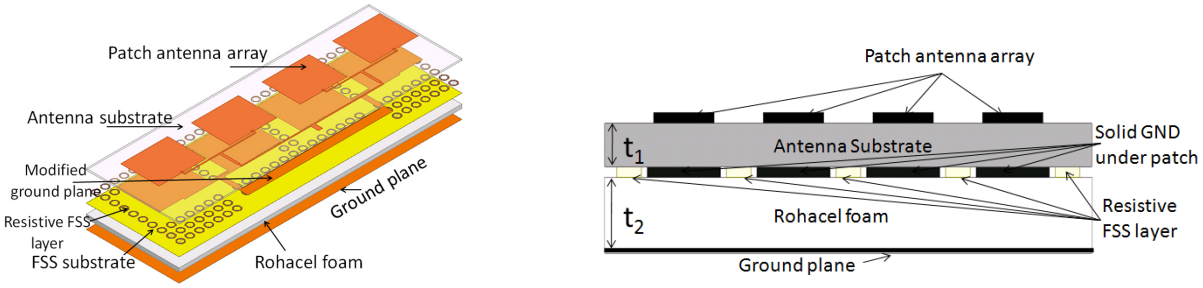

Figure 5. (a) Dielectric profile. (b) Schematic of the low RCS MSPAA with thin and wideband RAS.

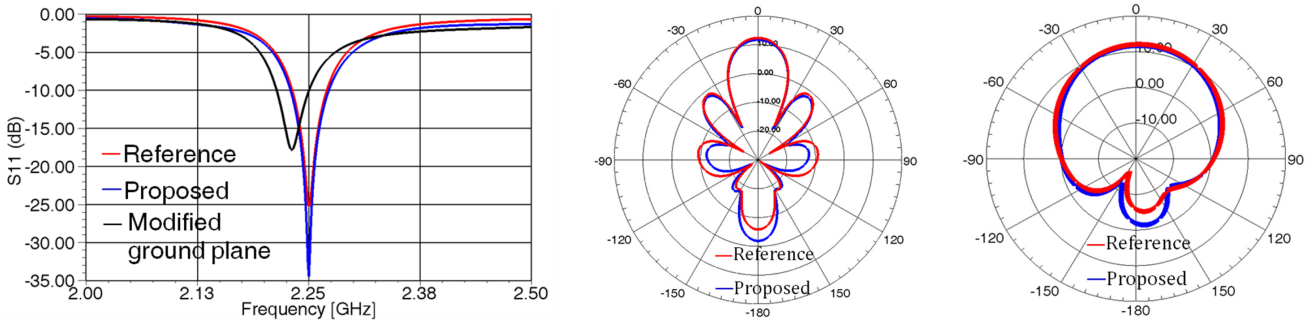

Figure 6. Simulated S_{11} and radiation patterns of MSPAA. (a) S_{11}, (b) E plane, (c) H plane.

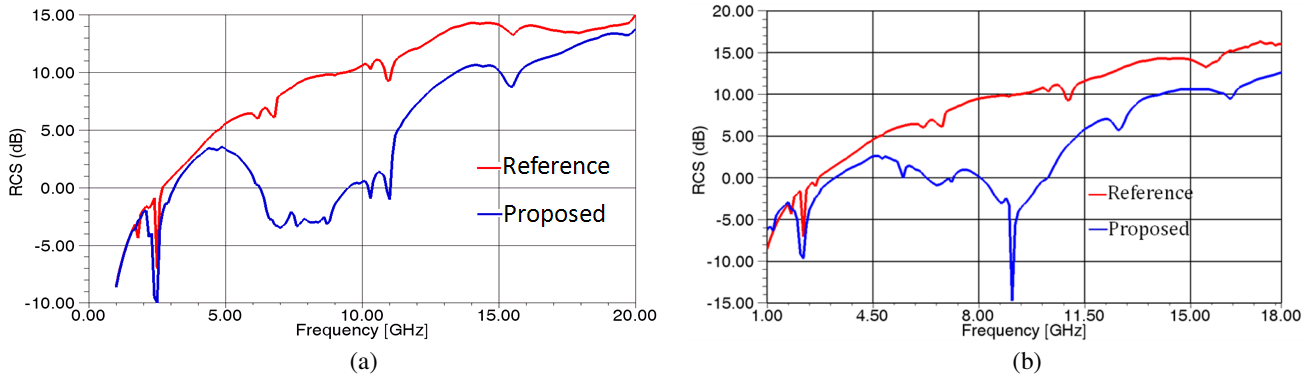

Figure 7. Simulated RCS of the MSPAA. (a) TM incidence. (b) TE incidence.

i. The resistive FSS layer and RAS are designed first, with constraints on the minimum thickness which would result in the desired wideband RCSR, to ensure its application as a primary stealth structure, *covering the entire air vehicle skins*. The antenna is designed next and optimized for *siting it atop the RAS*. The ground plane is modified so that unit cells can be fitted in the etched portion of the MGP, without increasing the PCB real estate of the reference antenna.

ii. Hence, with the optimized RAS design realized initially, meeting all the desired requirements, the antenna ground plane has been only modified for realizing the desired performance. It is observed that the MGP of the MSPAA does not result in any degradation in the reference antenna performance.

iii. In the RAS design, an antenna substrate of thickness 1.6 mm is incorporated into the design as a superstrate with the same material properties, so that the desired low RCS performance of the MSPAA with the RAS underneath is realized. Otherwise, the reference antenna placed on top of RAS

would not be expected to perform as desired.

iv. The modified ground plane of the proposed MSPAA, comprising solid ground beneath the patches and the feed lines yields the intended performance of the MSPAA without deteriorating either the impedance matching or the radiation performance of the antenna.

v. The resistive FSS layer, which is based on SOL FSS geometry with integral resistors, results in significant improvement in reliability, with no increase in the PCB real estate, thus rendering the design application worthy on any stealth platform.

vi. The radar absorber, designed and implemented as a thin and wideband radar absorbing structure, can be used independently as structural RAS and as skins of a stealthy UAV, and the low RCS conformal antenna can be seamlessly integrated into the skin with no protuberances or modifications to the existing stealth design with primary external shaping. Also, the Rohacel foam being a closed cell, flight worthy, low loss material can be used as the dielectric spacer with the required structural properties. It is observed that the RA design and implementation on any stealth platform demands multi-disciplinary inputs from structures and materials. The conducting ground plane of the RA can be easily replaced by using carbon fiber reinforced plastic (CFRP) with absolutely no loss in RCS performance of the conducting back plane and better structural characteristics. Monostatic RCS experiments performed earlier on similar size CFRP and Aluminium panels in a compact RCS test range showed that the RCS of CFRP and aluminium panels were matching both in amplitude and angle differing to the tune of 0.2 dB. The superstrate could be designed using glass fiber reinforced plastic (GFRP) meeting the required structural strength and also radar transparency, while meeting all RCSR requirements of RAS. Hence, the thin and wideband RAS can be used as a multi-functional UAV structure while satisfying stealth characteristics.

4. FABRICATION AND RCS MEASUREMENTS OF LOW RCS MICROSTRIP PATCH ANTENNA

The developed reference (1×4) MSPAA is shown in Fig. 8(a), and the MGP of the antenna array is shown in Fig. 8(b). The SOL FSS based resistive FSS PCB layer is designed using an ECAD PCB layout design software and is fabricated as a 5 mils thick PCB on an FR4 substrate, using a 50 Ω/sq resistive sheet. 'Selective etching' is carried out for etching the embedded passives resistors. The fabricated resistive FSS PCB layer of the low RCS MSPAA is shown in Fig. 9, and a zoomed unit cell is given in the inset of the same figure. The resistive FSS layer is assembled with a Rohacel foam layer of thickness 4 mm, and a tin plated 3 M conducting copper foil is used as the conducting ground plane of RA. The assembled low RCS MSPAA is shown in Fig. 10. The total thickness of low RCS MSPAA is 5.6 mm.

S_{11} measurements are carried out on the low RCS MSPAA using vector network analyzer, and the results are plotted in Fig. 11(a). It is once again observed from the figure that the measured S_{11} of the proposed MSPAA with RAS is *better* than the reference antenna. Matching results were obtained in simulation, indicating good agreement between simulation and experiments. The measurements of radiation pattern are carried out in microwave anechoic chamber. The measured E- and H-plane radiation patterns of the reference and proposed MSPAA are plotted in Figs. 11 (b) and 11(c), respectively. The measured gain in E- and H-planes is 11.8 dBi compared to 12 dBi gain in simulation.

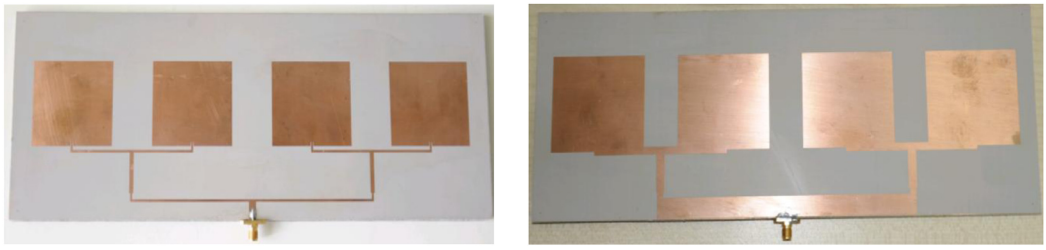

(a) (b)

Figure 8. (a) Top view of the (1×4) microstrip antenna array. (b) Modified ground plane of the low RCS microstrip antenna array.

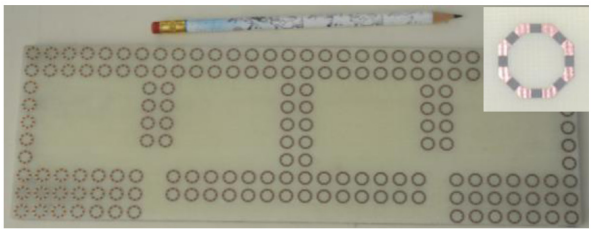

Figure 9. Photograph of the resistive layer. The area underneath the MGP of MSPAA is unfilled. *Inset: Zoomed single Octagonal resistive FSS element.*

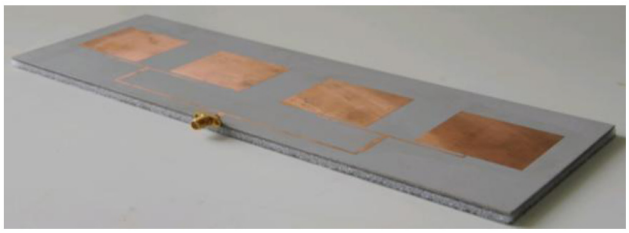

Figure 10. The proposed Low RCS microstrip antenna array with radar absorber.

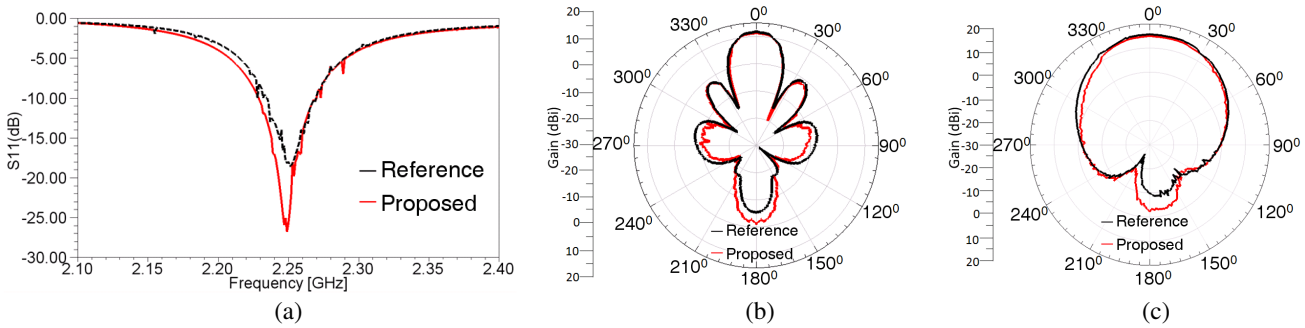

Figure 11. Measured S_{11} and radiation patterns of MSPAA. (a) S_{11}, (b) E plane, (c) H plane.

Figure 12. RCS measurements of low RCS MSPAA.

The very marginal difference in gain is attributed to fabrication and measurement tolerances and can be ignored.

RCS measurements of the reference antenna and the low RCS MSPAA are carried out in microwave anechoic chamber. The RCS measurement setup is shown in Fig. 12. Comparison plots of RCS of the reference and proposed low RCS antennas for both TE and TM incidences are plotted in Figs. 13(a), (b).

In a 'pseudo' monostatic RCS measurement setup, two high directivity horn antennas, one for transmission and the other for reception are well isolated from each other and located very closely with a bistatic angle of almost zero degrees. An analog phase shifter and attenuator in the coupled ports of the two directional couplers connected to the two horn antennas enable 'vectorial cancellation' of the RF background, at each measurement frequency, in the microwave anechoic chamber. The antenna is placed on a single axis positioner, enabling rotation in azimuth plane. RCS measurement results of the reference and proposed antenna are plotted in Figs. 13(a) and 13(b), for vertical and horizontal polarizations. It is observed that the simulated and measured RCS results agree well and indicate accurate simulation and also reliable translation of design to hardware using standard fabrication technology.

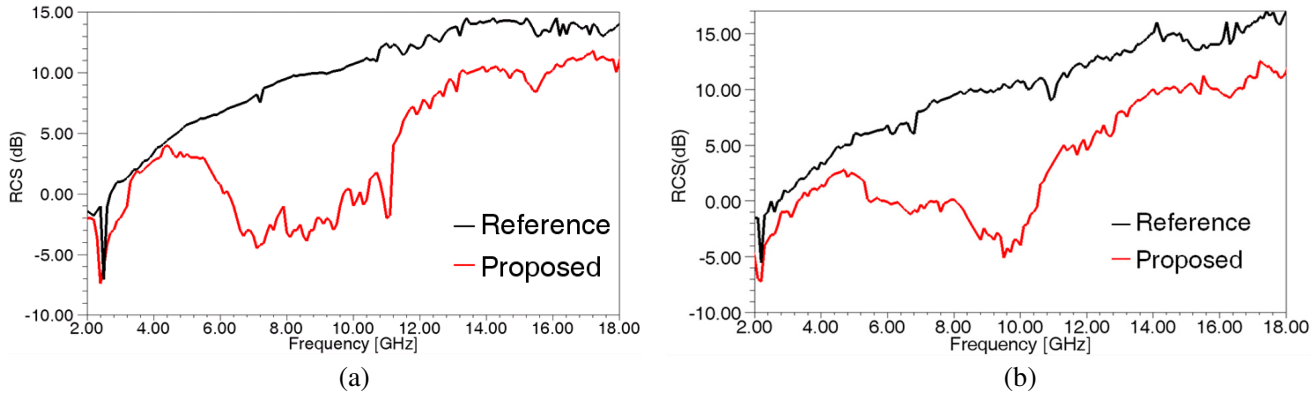

Figure 13. Measured RCS of the MSPAA. (a) TM incidence. (b) TE incidence.

5. CONCLUSION

A novel (1×4) low RCS microstrip antenna array with measured *out-of-band* RCSR of 5 dB to 15 dB from 6 GHz to 18 GHz is realized using thin and wideband radar absorbing structure, with no degradation in the radiation performance of the antenna. Resistors crucial in realizing resistive FSS layer of radar absorber are implemented as embedded passives resistors, which has resulted in significant improvement in RCSR performance. RCSR bandwidth can be further improved by using multi-layer RAS. The profile of the thin and wideband RA enables its application directly as skins of an air vehicle LO platform. The effort in this paper is focused on the reduction of RCS of a MSAA on an LO platform where the primary external shape design for radar LO is already in place, with radar absorbers designed and implemented as radar absorbing structure (RAS). The thin and wideband radar absorber is independently suited for applications in an air-vehicle stealth platform as a load bearing radar absorbing structure, which has been designed considering the inputs from structures and materials.

ACKNOWLEDGMENT

The authors gratefully thank the support and encouragement by Shri. MVKV Prasad, Outstanding Scientist and Director, ADE. We thank Shri. Dilip Y, Scientist G and Group Director for his continued support and guidance. We also thank Dr. Ramachandra, Sc. G and Group Director, FTTT and Shri. Diptiman Biswas, Sc. F, FTTT for providing the antenna and RCS measurement facility.

REFERENCES

1. Salisbury, W. W., "U.S. Patent, Absorbent body for electromagnetic waves," No. 2599944, 1952.
2. Eugene, F. K., F. J. Shaeffer, and M. T. Tuley, *Radar Cross Section*, 2nd edition, 9–10, Artech House, Norwood, MA, USA, 1993.
3. Munk, B., P. Munk, and J. Prior, "On designing Jaumann and circuit analog absorbers for oblique angle of incidence," *IEEE Trans. Antennas Propag.*, Vol. 55, No. 1, 2007.
4. Sudhendra, C., V. Mahule, A. C. R. Pillai, A. K. Mohanty, and K. Rao, "Novel embedded passives resistor grid network based wideband radar absorber," *IEEE Intl. Conf. on Elect., Computing and Comm. Technologies — IEEE CONECCT*, 1–4, DOI: 10.1109/CONECCT 2014.6740359, 2014.
5. Zadeh, A. K. and A. Karlsson, "Capacitive circuit method for fast and efficient design of wideband radar absorbers," *IEEE Trans. Antennas Propag.*, Vol. 57, No. 8, 2307–2314, Aug. 2009.
6. Costa, F. and A. Monorchio, "Electromagnetic absorbers based on high-impedance surfaces: From ultra-narrowband to ultra-wideband absorption," *Advanced Electromagnetics*, Vol. 1, No. 3, Oct. 2012.

7. Silva, M. W. B., A. L. P. S. Campos, and L. C. Kretly, "Design of thin microwave absorbers using lossy frequency selective surfaces," *Microw. Opt. Technol. Lett.*, Vol. 57, No. 4, Apr. 2015.
8. Hansen, R. C., "Relationships between antennas as scatterers and radiators," *Proc. IEEE*, Vol. 77, No. 5, 659–662, May 1989.
9. Genovesi, S., F. Costa, and A. Monorchio, "Low-profile array with reduced radar cross section by using hybrid frequency selective surfaces," *IEEE Trans. Antennas Propag.*, Vol. 60, No. 5, 2327–2335, May 2012.
10. Zheng, J., S. Fang, Y. Jia, and Y. Liu, "RCS reduction of patch array antenna by complementary split-ring resonators structure," *Progress In Electromagnetics Research C*, Vol. 51, 95–101, 2014.
11. Joozdani, M. Z., M. K. Amirhosseini, and A. Abdolali, "Wideband radar cross-section of patch array antenna with miniaturised hexagonal loop frequency selective surface," *Electron. Lett.*, Vol. 52, No. 9, 767–768, Apr. 2016.
12. Hao, Y., Y. Liu, K. Li, and S. Gong, "Wide band radar cross section reduction of microstrip patch antenna with split-ring resonators," *Electron. Lett.*, Vol. 51, No. 20, 1608–1609, Oct. 2015.
13. Liu, Y., Y. Hao, H. Wang, K. Li, and S. Gong, "Low RCS microstrip patch antenna using frequency-selective surface and microstrip resonator," *IEEE Antennas Wireless Propag. Lett.*, Vol. 14, 1290–1293, Feb. 2015.
14. Jia, Y., Y. Liu, H. Wang, and S. Gong, "Low RCS microstrip antenna using polarization-dependent frequency selective surface," *Electron. Lett.*, Vol. 50, No. 14, 978–979, 2014.
15. He, W., R. Jin, and J. Geng, "Low radar cross-section and high performances of microstrip antenna using fractal uniplanar compact electromagnetic band gap ground," *IEEE Microw., Antennas Propag.*, Vol. 1, No. 5, 986–991, 2007.
16. Miao, Z., C. Huang, X. Ma, M. Pu, X. Ma, Q. Zhao, and X. Luo, "Design of a patch antenna with dual-band radar cross section reduction," *Microw. Opt. Technol. Lett.*, Vol. 54, No. 11, 2516–2520, Nov. 2012.
17. Zhao, Y., X. Cao, J. Gao, X. Yao, T. Liu, W. Li, and S. Li, "Broadband metamaterial surface for antenna RCS reduction and gain enhancement," *IEEE Trans. Antennas Propag.*, early access, 2015.
18. Chen, Q. and Y. Fu, "A planar stealthy antenna Radome using absorptive frequency selective surface," *Microw. Opt. Technol. Lett.*, Vol. 56, No. 8, 1788–1792, 2014.
19. Huang, C., W. Pan, X. Ma, and X. Luo, "A frequency reconfigurable directive antenna with wideband low-RCS property," *IEEE Trans. Antennas Propag.*, Vol. 64, No. 3, 1173–1178, Jan. 2016.
20. Liu, Y., Y. Hao, K. Li, and S. Gong, "Radar cross section reduction of a microstrip antenna based on polarization conversion metamaterial," *IEEE Antennas Wireless Propag. Lett.*, Vol. 15, 80–83, May 2015.
21. Zheng, Y.-J., J. Gao, X.-Y. Cao, S.-J. Li, and W.-Q. Lli, "Wideband RCS reduction and gain enhancement microstrip antenna using chessboard configuration superstrate," *Microw. Opt. Technol. Lett.*, Vol. 56, No. 8, 1788–1792, 2014.
22. Zheng, J. and S. Fang, "A new method for designing low RCS patch antenna using frequency selective surface," *Progress In Electromagnetics Research Letters*, Vol. 57, No. 7, 1738–1741, Jul. 2015.
23. Huang, C., W. Pan, X. Ma, B. Jiang, and X. Luo, "Wideband radar cross section reduction of a stacked patch array antenna using metasurface," *IEEE Antennas Wireless Propag. Lett.*, Vol. 14, 1369–1372, 2015.
24. Rozanov, K. N., "Ultimate thickness to bandwidth ratio of radar absorbers," *IEEE Trans. Antennas Propag.*, Vol. 48, No. 8, 1230–1234, Aug. 2000.